Bulletin of Electrical Engineering and Informatics
Vol. 14, No. 6, December 2025, pp. 4548~4564
ISSN: 2302-9285, DOI: 10.11591/eei.v14i6.10599

Dispersion compensation in single and multi-channel DWDM using chirped apodized fiber Bragg gratings

Kripa Kalkala Balakrishna[1], Gopalakrishna Murthy Chinnammahalli Ramappa[2], Karthik Palani[3]
[1]Department of Electronics and Communication Engineering, Cambridge Institute of Technology, Bengaluru, India
[2]Department of Electronics and Communication Engineering, K S School of Engineering and Management, Bengaluru, India
[3]Department of Information Science Engineering, Cambridge Institute of Technology, Affiliated to Visvesvaraya Technological University (VTU), Bengaluru, India

Article Info

Article history:

Received Apr 29, 2025
Revised Sep 9, 2025
Accepted Sep 27, 2025

Keywords:

Chromatic dispersion
Dense wavelength division multiplexing
Fiber Bragg grating
Optical communication
Single-mode fiber

ABSTRACT

Chromatic dispersion (CD) is a key limiting factor in long-haul optical fiber communication, particularly in multi-channel dense wavelength division multiplexing (DWDM) systems, where it introduces signal distortion and inter-symbol interference (ISI). This paper proposes a low-dispersion-offset compensation (LDOC) scheme employing Gaussian-apodized linear chirped fiber Bragg gratings (CFBGs) to enhance dispersion management in single and multi-channel DWDM optical fiber communication systems. Simulations were performed in OptiSystem 7.0 for 10 Gbps single-channel transmission over standard single-mode fiber (SSMF) spanning 110–210 km, and were extended to 4- and 8-channel DWDM systems with a 0.8 nm channel spacing. System performance was evaluated in terms of quality factor (Q-factor), bit error rate (BER), and eye height under varying fiber lengths, input powers, and chirp coefficients. The LDOC-enhanced CFBG achieved a Q-factor of 7.04 with a BER of 9.82×10^{-13} for single-channel transmission at 180 km, 13.83 with a BER of 5.57×10^{-41} for a 4-channel system at 150 km, and 7.56 with a BER of 7.76×10^{-11} for an 8-channel system at 150 km. These results confirm significant improvements compared to conventional CFBGs, demonstrating that the proposed LDOC-based approach is a compact and effective solution for next-generation metro-core, long-haul, DWDM, and 5G/6G optical networks.

Corresponding Author:

Karthik Palani
Department of Information Science Engineering, Cambridge Institute of Technology
Affiliated to Visvesvaraya Technological University (VTU)
K.R. Puram, Bengaluru-560036, Karnataka, India
Email: karthik.ise@cambridge.edu.in

1. INTRODUCTION

The rapid growth of data-driven applications has created a strong demand for high-speed, long-distance optical communication systems. Optical fiber technology, with its high capacity and cost efficiency, forms the backbone of modern telecommunication networks [1]. For long-haul transmission, single-mode fibers (SMFs) are predominantly deployed, while multimode fibers are typically reserved for shorter links. In dense wavelength division multiplexing (DWDM) systems, however, overall performance remains constrained by attenuation, chromatic dispersion (CD), and nonlinear optical effects [2].

CD a key limitation in SMFs, arises because different wavelengths propagate at slightly different velocities within the fiber. This results from wavelength-dependent refractive index variations (material dispersion) and the fiber's structural geometry (waveguide dispersion). Over long distances, CD leads to

pulse broadening, inter-symbol interference (ISI), and transmission quality degradation. While attenuation and noise also impair performance, these are effectively mitigated using erbium-doped fiber amplifiers (EDFAs), which provide gain across the C and L bands while maintaining typical Q-factors above 6 and bit error rate (BER) below 10^{-9}, the generally accepted thresholds for reliable optical transmission. Despite such amplification techniques, CD remains the dominant impairment in high-capacity SMF links, necessitating effective compensation strategies. The 1,550 nm window is widely used for long-distance, high-bandwidth transmission because of its low attenuation and EDFA compatibility [3]–[5]. Fiber selection also plays a critical role in DWDM performance. For instance, ITU-T G.655 fibers exhibit relatively low dispersion (2–6 ps/(nm·km)) but are more prone to nonlinear effects under a narrow channel spacing of 50 GHz. In contrast, G.652 fibers, with higher dispersion (~17 ps/(nm·km)), are often preferred in DWDM systems since they help suppress nonlinearities. Furthermore, DWDM networks follow ITU-T standardized channel spacing on a 100 GHz frequency grid (186–196 THz), ensuring compatibility and interoperability in commercial deployments [6].

Wavelength division multiplexing (WDM) enhances bandwidth by transmitting multiple wavelengths simultaneously through a SMF, whereas DWDM uses narrowly spaced channels to achieve ultra-high capacity and long-haul transmission. Despite the efficiency of modern optical transmission systems, CD remains a critical challenge, as it degrades signal quality over distance and necessitates effective compensation [7]. Traditional approaches, such as dispersion compensating fibers (DCFs), use large negative dispersion coefficients to counteract accumulated positive dispersion in SMFs but suffer from high insertion loss, bulky size, increased nonlinear effects, and higher costs [8], [9]. Fiber Bragg gratings (FBGs) overcome these limitations by providing a compact, low-loss solution with customizable dispersion profiles, making them ideal for modern high-capacity optical networks [10]. In particular, Gaussian-apodized linear chirped fiber Bragg gratings (CFBGs) suppress sidelobes and enhance the spectral response, while Gaussian or Bessel filters at the receiver further reduce noise, together delivering significant performance improvements in DWDM systems [11].

Advancements in femtosecond (fs) laser direct writing techniques have further expanded the scope of FBG fabrication. Wolf *et al.* [12] reported that recent fs laser direct-writing approaches, such as those applied to multicore FBGs, enable high spatial precision and spectral control, thereby facilitating the fabrication of multifunctional chirped and apodized FBGs. Similarly, Grebnev *et al.* [13] reported fs laser inscription of low-loss, high-reflectivity chirped gratings in fluoride and chalcogenide glass fibers, targeting mid-infrared applications through advancements in material purity, rare-earth doping, and enhanced power handling. Willer *et al.* [14] employed a point-by-point dual-path fs technique, achieving reflectivity exceeding 90% and side-mode suppression ratios (SMSR) beyond 13 dB. Additionally, Guo *et al.* [15] proposed an energy-regulated fs-laser inscription approach to realize customizable apodization profiles without the need for traditional phase masks. Further innovations include the development of chirped and tilted FBGs (CTFBGs) with broad bandwidths (~75 nm), enabling fine control over chirp rate and tilt angle for high-power applications. Fan *et al.* [16] and Li *et al.* [17] reported fabrication of robust CTFBGs using fs-laser direct writing, achieving minimal insertion losses (<0.03 dB) under high optical powers exceeding 4 kW, demonstrating their suitability for Raman filtering and high-power laser systems. Advanced FBG fabrication techniques enable compact, low-loss devices with customizable dispersion profiles, ideal for modern photonic systems. Our simulations suggest these gratings can enhance dispersion compensation (DC) in high-capacity networks.

Elsayed [18] analyzed a WDM–free space optics (FSO) system using modified on-off keying (OOK) with adaptive thresholding to mitigate crosstalk, turbulence, and amplified spontaneous emission (ASE) noise. However, their focus on wireless optical links and modulation-based mitigation does not address the core issue of CD in fibers for high-speed DWDM systems. Keti [19] proposed a linear CFBG for single-channel DC with a Q-factor of 29.554 over 40 km standard single-mode fiber (SSMF) but lacked analysis on DWDM scalability and dynamic parameters. Naguib *et al.* [20] achieved 50% sidelobe suppression with raised cosine apodized FBGs but did not include dynamic chirp control or DWDM scalability. Ali and Ibrahim [21] reported a Q-factor of 8.04 and BER of 3.49×10^{-16} in a 4-channel WDM system over 100 km using uniform fiber Bragg gratings (UFBGs), without chirp tuning or apodization. Ghosh and Priye [22] used cascaded CFBGs for 24-channel DWDM with BER $\leq10^{-23}$ over 100 km, but faced complexity and insertion loss issues, lacking chirp-power optimization. Hossain *et al.* [23] reported a Q-factor of 2.39 and BER of 7.32×10^{-3} for a 100 km single-channel SMF link using Tanh-apodized CFBGs at 10 Gbps, limiting DWDM use.

Prior studies have mainly focused on static CFBG configurations and traditional DCFs with limited scalability, typically in single-channel systems over distances below 110 km. In contrast, this work presents a dynamically optimized Gaussian-apodized linear CFBG with adaptive chirp and power tuning, extending transmission reach up to 180 km for single-channel and 150 km for multi-channel DWDM systems. Despite

these advances, dynamic optimization of key parameters such as chirp, input power, and fiber length remains underexplored, especially for long-haul (>110 km) DWDM applications.

This work overcomes limitations of prior studies by proposing a dynamically optimized Gaussian-apodized linear CFBG-based low-dispersion-offset compensation (LDOC) scheme for DC in single- and multi-channel DWDM systems. Unlike static CFBG or bulky DCF methods, it adaptively tunes chirp coefficients and input power to enhance Q-factor and BER. The scheme extends transmission reach up to 180 km in single-channel systems, achieving a Q-factor of 7.04 and a BER of 9.82×10^{-13}. It demonstrates scalability in 4- and 8-channel DWDM over 150 km SSMF, with Q-factors of 13.83 and 7.56 and BERs of 5.57×10^{-41} and 7.76×10^{-11}, respectively. This approach reduces system complexity and insertion loss by eliminating cascaded CFBGs and DCF modules, thereby providing a compact and cost-effective solution for long-haul optical networks. We developed a reproducible Optisystem 7.0 simulation workflow to systematically validate chirp, input power, and apodization optimizations, filling key gaps overlooked in earlier studies.

2. BASICS OF FIBER BRAGG GRATING

A FBG is a section of optical fiber where the core's refractive index is periodically varied. This modulation is typically created by exposing a photosensitive fiber core to an interference pattern of ultraviolet light. When light propagates through the grating, part of it is reflected and the rest continues forward, a phenomenon explained by Fresnel reflection at index boundaries. The simplest type, the UFBG, has evenly spaced periodic index variations [24].

2.1. Chirped fiber Bragg grating

CFBGs are an advanced form of FBG characterized by a non-uniform grating period, as illustrated in Figure 1. This design enables reflection over a broad wavelength range, with each wavelength experiencing a unique time delay. The stretched optical pulse from the dispersive fiber enters the CFBG through a circulator. The grating period of CFBG varies linearly, so different wavelengths are reflected at various positions. long wavelengths (delayed more in the fiber) are reflected earlier, while short wavelengths (delayed less) are reflected later. This opposite delay counteracts the fiber's dispersion, compressing the broadened pulse back to its original shape. Thus, the CFBG effectively compensates for dispersion.

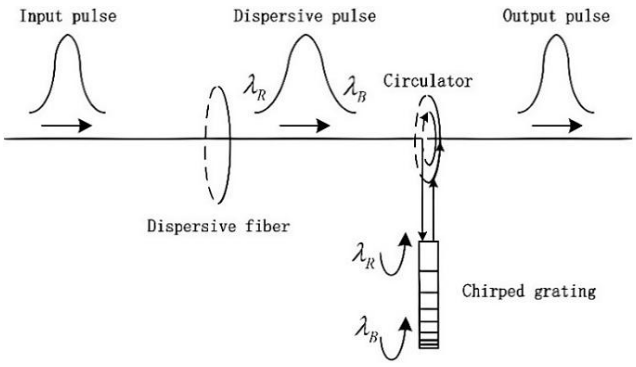

Figure 1. Operating principle of a CFBG: reflects specific wavelengths λ_R while transmitting others [25]

2.2. Theoretical study of chirped fiber Bragg grating

Each segment of a CFBG reflects wavelengths that satisfy the Bragg condition, which defines the wavelength λ_B at which total internal reflection occurs, as (1). The refractive index distribution n(z) of the CFBG is described by (2). The fundamental design relations of CFBGs, including Bragg wavelength, index distribution, chirp, and grating period, are adapted from [26].

$$\lambda_B = 2\, n(z)\, \Lambda(z) \tag{1}$$

$$n\,(z) = n_{eff} + \Delta n\, g(z)\, cos\,\{\frac{2\pi z}{\Lambda 0}\,(1 + x\,(z)\} \tag{2}$$

In this context, n_{eff} denotes the effective refractive index, x represents the grating's linear chirp, Δn is the refractive index modulation, and g(z) corresponds to the apodization profile. The chirp Δλ, given (3), represents the wavelength difference between λ_{Long} (longest) and λ_{Short} (shortest).

$$\Delta\lambda = 2n_{eff}\ (\Lambda_{Long} - \Lambda_{Short}) \quad (3)$$

The spacing between grating planes along the core is calculated using (4). Where the grating period is Λ_0 at the midpoint and z is the position along the CFBG. This variation imparts a unique delay to each wavelength.

$$\Lambda\ (z) = \Lambda_0\ +\ x\ z \quad (4)$$

3. METHOD

This work proposes a LDOC scheme based on Gaussian-apodized linear CFBGs to mitigate CD in single- and multi-channel DWDM systems operating at 10 Gbps, as shown in Figure 2. Unlike conventional DCF or fixed-length CFBG approaches, the proposed method jointly optimizes the apodization profile and chirp coefficient, enabling flexible, low-penalty performance over long-haul links. The system was modeled and simulated in Optisystem 7.0 for single-channel, 4-channel, and 8-channel DWDM configurations. In the single-channel system, performance was assessed by examining the Q-factor, eye height, and BER across different SSMF lengths (110–210 km), input powers (0–20 dBm), and chirp coefficients (0.00001–0.01 μm). For DWDM configurations, additional analysis was performed by varying SSMF length and chirp parameters across different channel frequencies. The component parameters are summarized in Table 1.

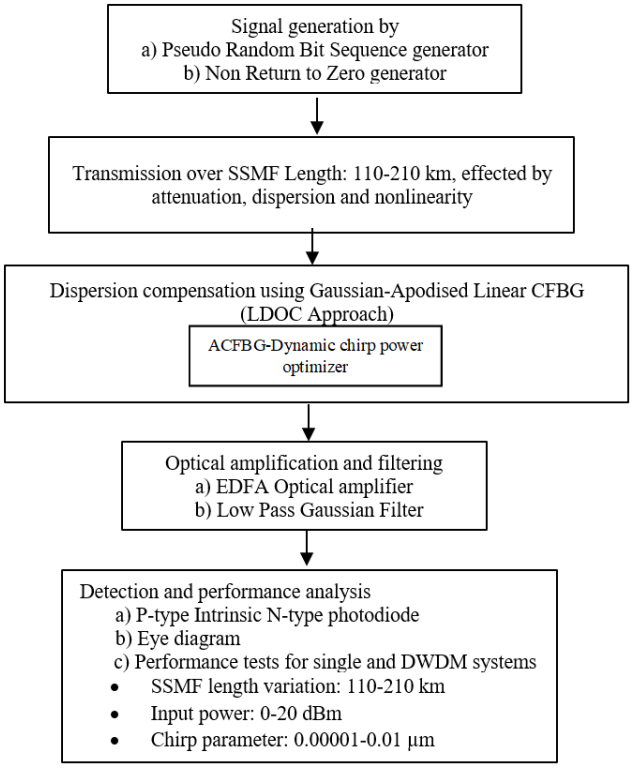

Figure 2. Flowchart of the proposed LDOC-based DWDM system methodology

The simulation parameters were chosen to model long-haul DWDM links in Optisystem 7.0 using ITU-T G.652 SSMF with in-line DC. Fiber spans were selected to represent typical metro-core and long-haul networks, ranging from 110–210 km for single-channel systems, 110–200 km for 4-channel DWDM, and up to 150 km for 8-channel DWDM configurations, where in-line compensation is required to counteract accumulated dispersion before optical signal regeneration. Channel allocation followed the ITU-T G.694.1 DWDM frequency grid with 100 GHz spacing, ensuring seamless compatibility with standard DWDM systems.

Input power for the single-channel system was varied between 0 and 20 dBm, typical for long-haul links, to examine the impact of nonlinear impairments on optical signal-to-noise ratio (OSNR) performance, while DWDM systems used a fixed 10 dBm to prevent inter-channel effects. The CFBG chirp parameter was swept from 0.00001 to 0.01 μm in single-channel links to enable full DC over long spans, while a narrower range of 0.00001–0.001 μm was used in DWDM systems to optimize slope matching. A linear chirp ensured predictable wavelength-dependent delay, while Gaussian apodization (Gauss=0.5) reduced sidelobes and insertion loss. In-line EDFAs with 20 dB gain and a 4 dB noise figure compensated for fiber loss while limiting ASE noise. System performance was evaluated in terms of Q-factor, BER, and eye height.

Table 1. Simulation components and their parameters

Components	Parameters
Pseudorandom bit sequence (PRBS) generator	Data rate: 10 Gbps
Non-return-to-zero (NRZ) pulse generator	Duty cycle: 0.5
Continuous wave (CW) laser	Input power: varying from 0 dBm to 20 dBm
	Line width: 0.01 MHz
	Channel central frequency for single channel: 193.4 THz
	Channel central frequency for 4 channels: 193.1 THz to 193.4 THz
	Channel central frequency for 8 channels: 193.1 THz to 193.8 THz
Mach-zehnder modulator (MZM)	Extinction ratio: 30 dB
Standard SMF-28	Length: varying from 110 km to 210 km
	Attenuation loss: 0.18 dB/km
	Dispersion: 16.5 ps/nm/km
	Dispersion slope: 0.05 ps/nm^2/km
	Core effective area: 76.5 μm^2
FBG	Length: 30 mm
	Effective index: 1.45
	Apodization function: Gaussian
	Gauss parameter: 0.5
	Chirp function: linear
	Linear parameter: varying from 0.00001 μm to 0.01 μm
EDFA optical amplifier	Gain: 20 dB
	Noise figure: 4 dB
P-type intrinsic N-type (PIN) photodetector	Responsivity: 1 A/W
	Dark current: 10 nA
Low-pass Gaussian (LPG) filter	Cutoff frequency: 0.75×bit rate

3.1. Single-channel low-dispersion-offset compensation-based optical communication system

The single-channel LDOC system, illustrated in Figure 3, comprises three main sections: the transmitter, the SSMF transmission link, and the receiver. The transmitter includes a PRBS generator operating at 10 Gbps, followed by an NRZ pulse generator that controls bandwidth and shapes the electrical pulses. Modulation is performed using an MZM with a 30 dB extinction ratio, driven by a CW laser operating at 193.4 THz with a power output ranging between 0–20 dBm. The modulated optical signal travels through the SSMF link, varied between 110–210 km, with Gaussian-apodized linear CFBGs placed symmetrically before and after the SSMF to compensate for accumulated CD. EDFA optical amplifiers are incorporated after the apodized CFBG (ACFBG) module to amplify the signal, ensuring adequate power levels without excessive noise figure penalties. At the receiver, a PIN photodetector transforms the optical signal into an electrical signal, which is then passed through a low-pass Gaussian filter to remove high-frequency noise. A 3R regenerator restores the signal quality, and performance is evaluated using eye diagrams, focusing on Q-factor, eye height, and BER.

3.2. Low-dispersion-offset compensation-based dense wavelength division multiplexing systems: 4 and 8 channels configurations

The proposed LDOC-based DWDM system architecture, depicted in Figure 4, extends the DC approach to multi-channel systems with 4-channel and 8-channel configurations. The system structure includes the transmitter, SSMF transmission link, and receiver. The N-channel transmitter comprises a PRBS generator for data scrambling, an NRZ pulse generator for pulse shaping and bandwidth control, and a CW laser diode that provides 10 dBm optical carriers. For the 4-channel DWDM system, the carrier frequencies range from 193.1 THz to 193.4 THz. For the 8-channel configuration, the frequency span extends to 193.8 THz, with a channel bandwidth of 80 GHz. The optical carriers are modulated using an MZM with a 30 dB extinction ratio, and an N:1 DWDM multiplexer combines the channels for parallel transmission over the SSMF.

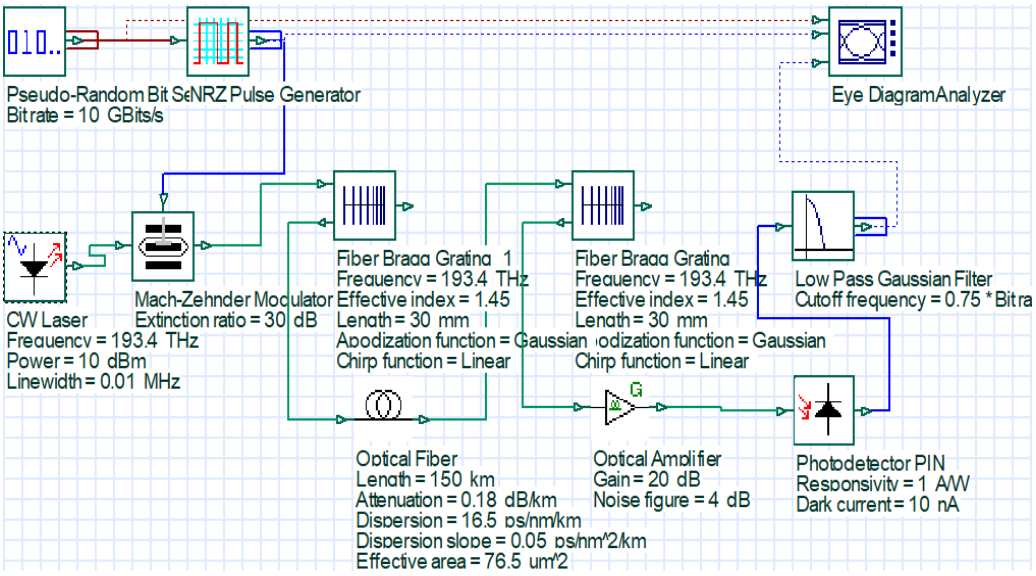

Figure 3. Simulation design of the proposed LDOC scheme for a single-channel system

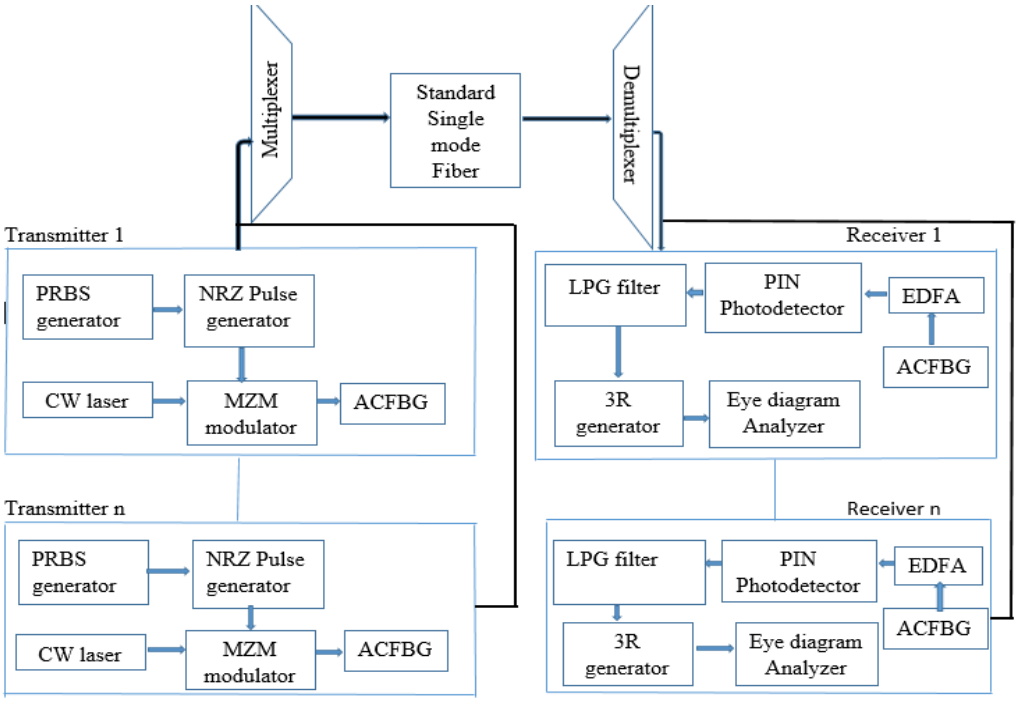

Figure 4. Functional diagram of the proposed LDOC architecture in a DWDM system

CD is compensated using Gaussian-apodized linear CFBGs, placed symmetrically before and after the DWDM multiplexer and de-multiplexer to ensure optimal dispersion management across all channels. At the receiver, a 1: N DWDM de-multiplexer separates the aggregated signal into individual channels. Each channel is then amplified using an EDFA, converted to the electrical domain via a PIN photodetector, and filtered through an LPG Filter to remove residual noise. Finally, a 3R regenerator restores signal quality, and system performance is evaluated using an eye diagram analyzer.

The simulation setups for the 4-channel and 8-channel DWDM configurations are shown in Figures 5 and 6, respectively. They depict the transmitter, transmission fiber, and receiver structure, as implemented in Optisystem 7.0.

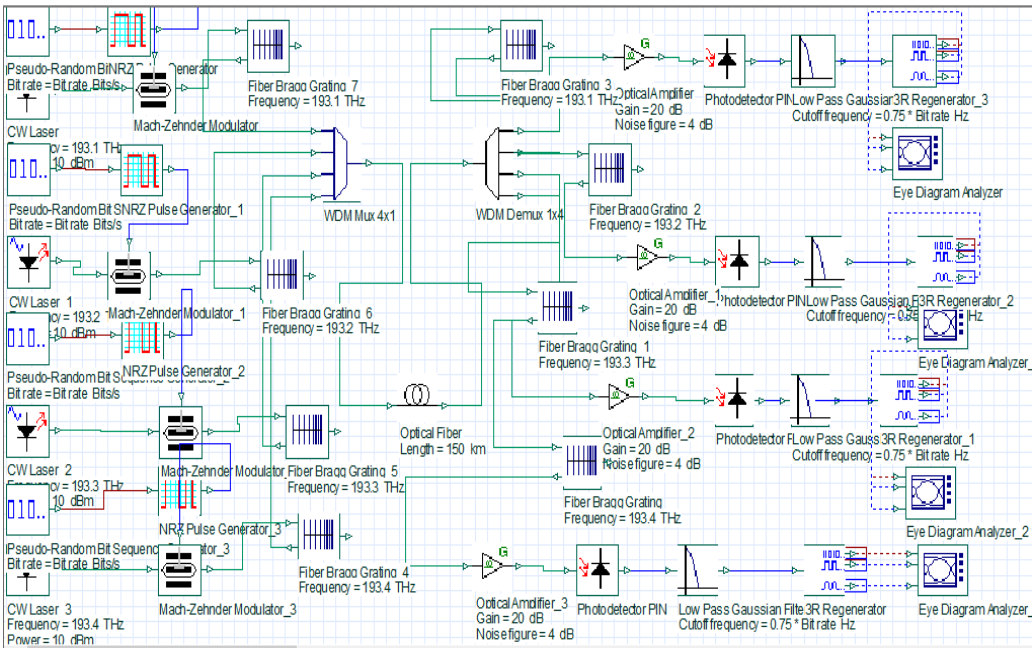

Figure 5. Simulation configuration of the 4-channel DWDM system

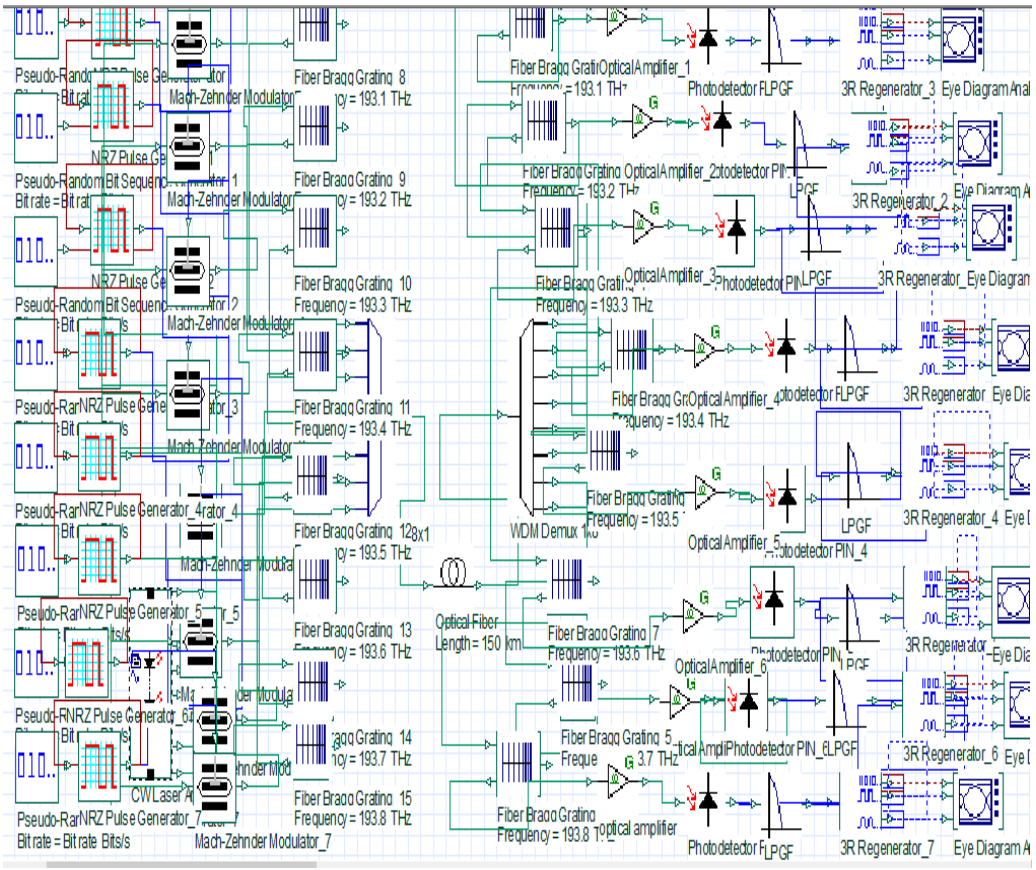

Figure 6. Simulation framework for the 8-channel DWDM system

4. RESULTS AND DISCUSSION

This study evaluates and compares 4- and 8-channel DWDM systems over 110–200 km fiber links at 10 Gbps, employing LDOC with a Gaussian-apodized linear CFBG for DC. For baseline comparison, a

single-channel system is analyzed by varying the SSMF length from 110 km to 210 km, input power from 0 dBm to 20 dBm, and chirp parameters from 0.00001 μm to 0.01 μm. The system is evaluated based on Q-factor, BER, and eye height. In a CFBG, different wavelengths reflect at different grating positions, causing a wavelength-dependent delay τ(λ) as expressed in (5), where c is the speed of light and l indicates the FBG length. The dispersion, essential for compensating the positive CD of the SSMF, is obtained by differentiating τ(λ) with respect to λ, which yields the linear group delay variation in (6). These relations are adapted from [26].

$$\tau(\lambda) = (\lambda_B - \lambda)\frac{2neffl}{c} \tag{5}$$

$$D_g = \frac{d\tau(\lambda)}{d\lambda} = \frac{2neffl}{\Delta\lambda c} \tag{6}$$

To ensure effective DC across the transmission link, the total system dispersion must satisfy the matching condition expressed in (7) [27]:

$$D_{SSMF} \cdot L_{fiber} + D_{FBG} = 0 \tag{7}$$

Where, D_{SSMF} is the dispersion parameter of the SSMF, L_{fiber} is the SSMF length, and D_{FBG} represents the dispersion introduced by the FBG. For effective DC, the negative dispersion introduced by the CFBG in (8) must precisely offset the accumulated positive dispersion of the SSMF, thereby fulfilling the matching condition in (7). The dispersion contributed by the CFBG is expressed as (8):

$$D_{FBG} = -\frac{2neffl}{c(\lambda L - \lambda s)} \tag{8}$$

as described in [28], proper chirp bandwidth design ($\lambda_L - \lambda_S$) enables CFBGs to provide negative dispersion, while Gaussian apodization reduces sidelobes by varying the refractive index along the grating, expressed in (9).

$$g\,(z) = exp\left(-a\left(\frac{z}{l} - 0.5\right)^2\right) \tag{9}$$

Q-factor and BER are inversely related exponentially. A mismatch in D_{FBG} dispersion reduces the Q-factor and increases the BER, while precise D_{FBG} tuning maintains a high Q-factor and minimizes BER. The Q-factor is calculated based on the OSNR, as defined in (10), where B_o denotes the optical filter bandwidth and B_c the receiver filter bandwidth.

$$Q = \frac{OSNR}{\sqrt{2.OSNR+1}+1}\sqrt{\frac{Bo}{Bc}} \tag{10}$$

Finally, the BER is expressed as a function of the Q-factor in (11):

$$BER \approx \frac{exp\,(\frac{-Q}{2})}{Q\sqrt{2\pi}} \tag{11}$$

With this theoretical foundation established, the following subsections present comparative simulation results.

4.1. Comparison between pure and apodized chirped fiber Bragg gratings

A comparative evaluation of transmission performance between a pure CFBG and a Gaussian-ACFBG in a single-channel system was conducted under identical conditions with an SSMF length of 150 km, an FBG length of 30 mm, and an input power of 10 dBm. The corresponding eye diagrams are presented in Figure 7, while the results are summarized in Table 2. Figure 7(a) shows that the pure CFBG suffered from strong sidelobes and poor spectral shaping, resulting in complete signal degradation with a Q-factor of 0, BER of 1, and eye height of 0. In contrast, Figure 7(b) demonstrates that the Gaussian-ACFBG achieved a Q-factor of 16.59, a BER of approximately 4.41×10^{-62}, and an eye height of 0.00135 with a wide-open eye diagram, confirming its highly effective DC capability.

The pure CFBG leads to complete signal failure, evidenced by a Q-factor of 0, a BER of 1, and an eye height of 0. In contrast, the Gaussian-ACFBG achieves a Q-factor of 16.59, an extremely low BER of

approximately 4.41×10^{-62}, and an eye height of 0.00135, indicating strong signal quality and reliable transmission. Thus, Gaussian apodization suppresses sidelobes and smooths the reflectivity profile, reducing distortion, and enabling superior long-distance performance compared to pure CFBGs.

Table 2. Comparative analysis of pure CFBG and ACFBG

FBG type	Q-factor	BER	Eye height
Pure CFBG	0	1	0
ACFBG	16.5859	4.40737e-062	0.00135016

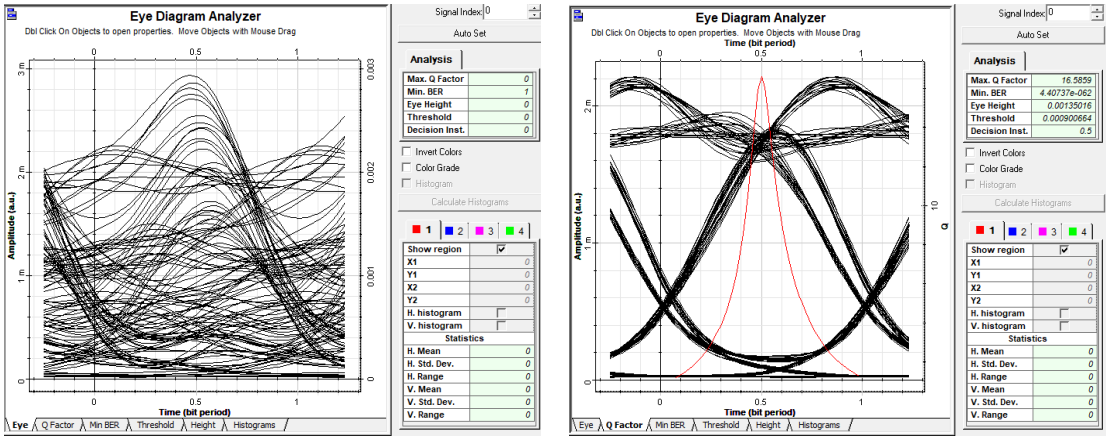

Figure 7. Eye diagrams; (a) pure CFBG with signal failure (Q-factor=0, BER=1, and eye height=0) and (b) ACFBG with high performance (Q-factor=16.59, BER≈4.41×10^{-62}, eye height=0.00135)

4.2. Effect of varying standard single-mode fiber length on the proposed optical system performance

This study investigates single-channel 10 Gbps transmission over 110–210 km of SSMF using a 30 mm FBG length with an input power of 10 dBm. The corresponding eye diagrams at different transmission distances are shown in Figure 8, while the overall results are summarized in Table 3. At 110 km, shown in Figure 8(a), the system performs optimally with a Q-factor of 38.73, BER≈0, and an eye height of 0.0082. At 150 km, Figure 8(b) shows that dispersion reduces the Q-factor to 16.59 and the eye height to 0.00135, with BER≈4.41×10^{-62}. At 180 km, Figure 8(c) indicates further degradation, with a Q-factor of 7.04, BER≈9.82×10^{-13}, and an eye height of 0.00023. By 210 km, Figure 8(d) reveals severe distortion, resulting in a Q-factor of 2.62, BER≈0.0044, and a nearly closed eye height of -1.41×10^{-5}.

Table 3. Performance evaluation for different SSMF lengths

SSMF length (km)	Q-factor	BER	Eye height
110	38.7341	0	0.0082486
120	33.7889	1.41E-250	0.00537562
130	25.0814	3.96E-139	0.0034501
140	19.856	4.88E-88	0.0021788
150	16.5859	4.41E-62	0.0013502
160	12.7171	2.38E-37	0.0007998
170	9.55157	6.39E-22	0.0004499
180	7.03681	9.82E-13	0.0002331
190	5.31973	5.18E-08	0.0001112
200	3.75731	8.59E-05	3.18E-05
210	2.61568	0.00444144	-1.41E-05

The system demonstrates excellent performance between 110 km and 130 km, with high Q-factors (greater than 25), extremely low BER, and wide eye openings, confirming highly reliable transmission. At 140–150 km, signal quality moderately degrades due to dispersion, though performance remains robust with Q-factors greater than 16. From 160 km to 180 km, further degradation is observed; however, the system still meets the minimum communication threshold (Q-factor>6). Beyond 180 km, the Q-factor drops below 6, the

BER rises sharply, and the eye diagram significantly narrows. By 210 km, the signal becomes severely distorted, with a Q-factor of 2.62 and a BER≈0.0044, indicating transmission failure. These results confirm that the maximum achievable SSMF length for acceptable transmission in a single-channel without additional DC is 180 km.

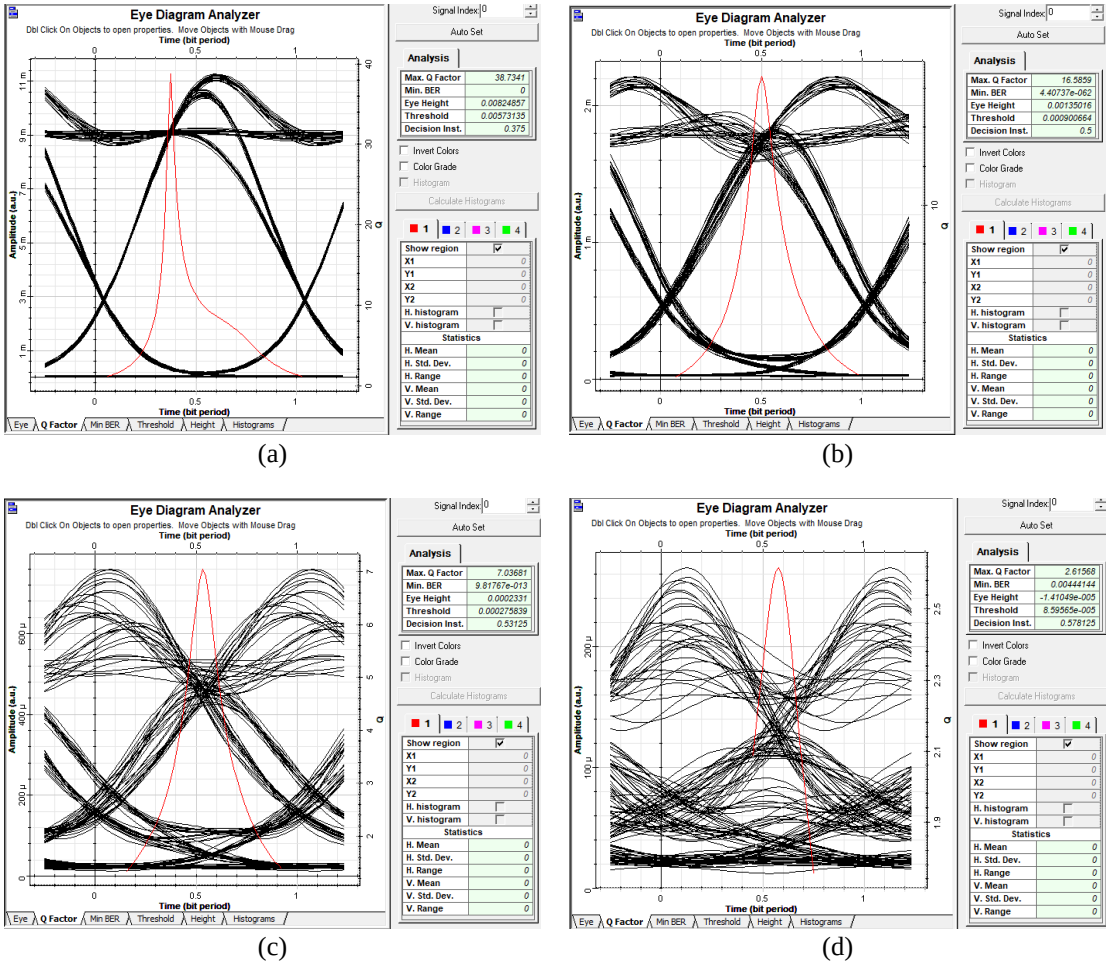

Figure 8. Eye diagrams for various SSMF lengths highlighting CD and signal deterioration; (a) at 110 km (Q-factor=38.73, BER=0, eye height=0.0082), (b) at 150 km (Q-factor=16.59, BER≈4.41×10^{-62}, eye height=0.00135), (c) at 180 km (Q-factor=7.04, BER≈9.82×10^{-13}, eye height=0.00023), and (d) at 210 km (Q-factor=2.62, BER≈0.0044, eye height=-1.41×10^{-5})

4.3. Impact of input power on the performance of the designed optical system

Figure 9 presents the impact of input power variation on system performance for a single-channel configuration with a 150 km SSMF and a 30 mm FBG length, with the detailed results summarized in Table 4. The input power is varied from 0 dBm to 20 dBm, and its effect is analyzed in terms of eye height, Q-factor, and BER to assess the quality of transmission. To illustrate the performance trend, two representative cases are discussed. At 0 dBm, as shown in Figure 9(a), the eye diagram is nearly closed, with an eye height of 0.0001, a Q-factor of 9.39, and a BER of 2.84×10^{-21}, indicating poor signal quality. At 10 dBm, Figure 9(b) shows a wide and clear eye with an eye height of 0.00135, a Q-factor of 16.59, and a BER of 4.41×10^{-62}, reflecting optimal performance and minimal dispersion.

The findings reveal that increasing input power from 0 dBm to 10 dBm steadily improves system performance. At 0 dBm, signal quality is poor, improves at 5 dBm, and peaks at 10 dBm with a Q-factor of 16.59, BER≈4.41×10^{-62}, and a clear eye diagram. Beyond 10 dBm, nonlinear effects become significant at 15 dBm, where the Q-factor drops and the BER increases. At 20 dBm, severe distortion occurs, resulting in a Q-factor of 0 and a BER of 1. Thus, 10 dBm is identified as the optimal input power, balancing signal strength and nonlinear degradation for long-distance optical transmission.

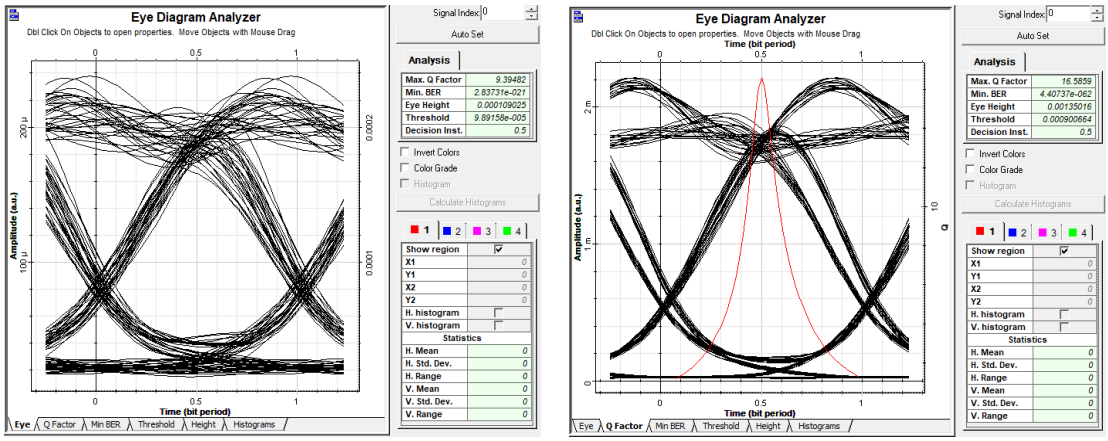

(a) (b)

Figure 9. Eye diagrams displaying the impact of input power variations on signal quality; (a) at 0 dBm–low Q-factor of 9.39, BER≈2.84×10^{-21}, eye height≈0.0001 and (b) at 10 dBm–improved signal quality with Q-factor of 16.59, extremely low BER≈4.41×10^{-62}, and wider eye height of 0.00135

Table 4. System performance for varying input power

Input power (dBm)	Q-factor	BER	Eye height
0	9.39482	2.83731e-021	0.000109025
5	13.2612	1.94092e-040	0.000394701
10	16.5859	4.40737e-062	0.00135016
15	10.4437	6.03201e-026	0.00381567
20	0	1	0

4.4. Linear chirp performance in single- and multi-channel dense wavelength division multiplexing over standard single-mode fiber lengths

The effect of varying the linear chirp coefficient (0.00001–0.01 µm) is analyzed for a single-channel system over 110, 150, and 200 km of SSMF with a 30 mm FBG length at an input power of 10 dBm. Eye diagrams for 110 km and 200 km are shown in Figure 10, and the results in Table 5 identify 0.0001 µm as the optimal chirp coefficient. Representative eye diagrams for this optimal case are shown in Figures 10(a) and (b). At 110 km in Figure 10(a), the system delivered excellent performance, achieving a Q-factor of 38.73, zero BER, and an eye height of 0.0082. At 200 km in Figure 10(b), although dispersion reduced signal quality, the same optimal chirp still provided the best results, with a Q-factor of 3.76, BER≈8.6×10^{-5}, and an eye height of 3.17×10^{-5}.

Single-channel performance strongly depends on the linear chirp and fiber length. A chirp of 0.0001 µm obtained superior performance, with a Q-factor of 38.7341 and BER of 0 at 110 km, and a Q-factor of 16.585 with a BER of 4.41×10^{-62} at 150 km, achieving error-free transmission up to 150 km and the lowest BER at 200 km. Other chirp values resulted in higher BER and lower Q-factors, particularly at longer distances.

Table 5. Impact of linear chirp parameter on single-channel performance

Linear chirp parameter (µm)	SSMF length (km)	Q-factor	BER	Eye height
0.00001	110	4.98805	2.53591e-007	0.00338634
0.0001	110	38.7341	0	0.00824857
0.001	110	4.50628	3.29869e-006	0.000229207
0.002	110	3.62088	0.000146791	3.3529e-005
0.01	110	0	1	0
0.00001	150	3.68608	0.000104811	0.000293139
0.0001	150	16.5859	4.40737e-062	0.00135016
0.001	150	0	1	0
0.002	150	0	1	0
0.01	150	0	1	0
0.00001	200	2.02256	0.0198156	-8.6952e-005
0.0001	200	3.75731	8.58514e-005	3.1775e-005
0.001	200	0	1	0
0.002	200	0	1	0
0.01	200	0	0	0

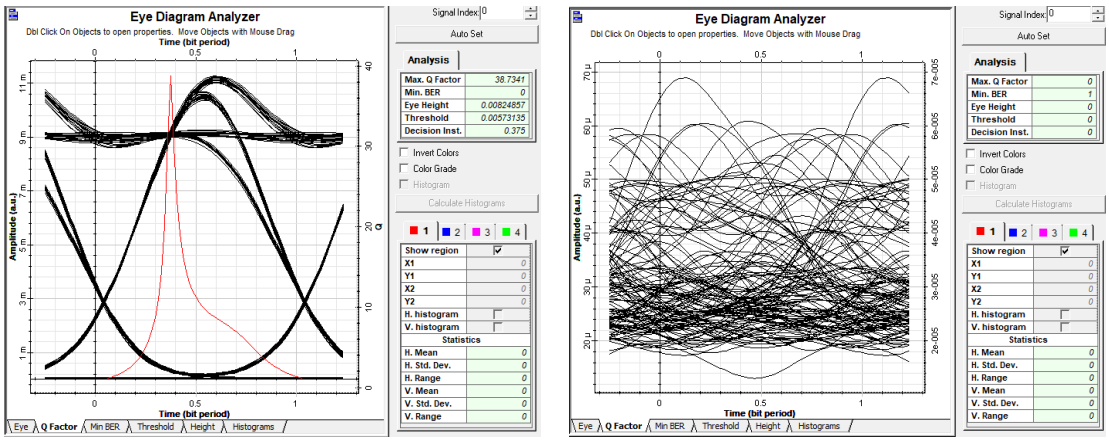

(a) (b)

Figure 10. Eye diagrams for a chirp of 0.0001 µm; (a) at 110 km–Q-factor is 38.73, BER of 0, eye height of 0.0082 and (b) at 200 km–Q-factor is 3.76, BER≈8.6×10^{-5}, eye height of 3.17×10^{-5}

Building on the single-channel analysis, three linear chirp values (0.00001 µm, 0.0001 µm, and 0.001 µm) were evaluated in a 4-channel DWDM system to assess their impact on Q-factor, BER, and eye height. The study covered channel frequencies from 193.1 to 193.4 THz and SSMF lengths of 110 km, 150 km, and 200 km, with results summarized in Table 6. The findings confirm that both chirp value and transmission distance critically influence system performance. Figure 11 illustrates Q-factor variation with channel frequency for the three chirp values, underscoring the importance of selecting an optimal chirp coefficient to maximize DWDM performance.

Table 6. Linear chirp parameter performance across SSMF lengths and channel frequencies in DWDM

Channel frequency (THz)	Linear chirp parameter (µm)	SSMF length (km)	Q-factor	BER	Eye height
193.1	0.00001	110	3.12819	0.000864022	0.000469605
193.2	0.00001	110	3.04041	0.00114017	0.000153795
193.3	0.00001	110	3.12055	0.000883899	0.000451173
193.4	0.00001	110	3.12971	0.000859679	0.000486938
193.1	0.00001	150	2.38531	0.00618829	-0.00046609
193.2	0.00001	150	2.40811	0.00573445	-0.000460555
193.3	0.00001	150	2.43593	0.00545083	-0.000426817
193.4	0.00001	150	3.043	0.00116087	3.01336e-005
193.1	0.00001	200	2.91227	0.00159975	-6.38121e-006
193.2	0.00001	200	3.30029	0.000449807	2.03346e-005
193.3	0.00001	200	3.32553	0.000405837	2.20931e-005
193.4	0.00001	200	0	1	0
193.1	0.0001	110	25.9996	2.38899e-149	0.00796097
193.2	0.0001	110	24.498	7.3932e-133	0.00796442
193.3	0.0001	110	21.7288	5.08243e-105	0.00774574
193.4	0.0001	110	28.0797	8.50795e-174	0.00797466
193.1	0.0001	150	13.586	2.39411e-042	0.00126343
193.2	0.0001	150	14.2489	2.25412e-046	0.00128783
193.3	0.0001	150	13.2495	2.22838e-040	0.00126481
193.4	0.0001	150	14.256	2.04361e-046	0.00129031
193.1	0.0001	200	2.78391	0.00207779	-1.73947e-005
193.2	0.0001	200	2.88157	0.00150832	-9.71651e-006
193.3	0.0001	200	2.86983	0.00162167	-1.06705e-005
193.4	0.0001	200	2.73253	0.00243693	-2.23292e-005
193.1	0.001	110	3.23844	0.000519796	6.75292e-005
193.2	0.001	110	3.30165	0.000418259	8.50085e-005
193.3	0.001	110	3.21627	0.000553504	6.29645e-005
193.4	0.001	110	3.16298	0.00066985	4.76408e-005
193.1	0.001	150	2.755	0.00264154	-1.38212e-005
193.2	0.001	150	2.82937	0.00185483	-1.06963e-005
193.3	0.001	150	2.75923	0.00236217	-1.27668e-005
193.4	0.001	150	2.74673	0.00238371	-1.6162e-005
193.1	0.001	200	0	1	0
193.2	0.001	200	0	1	0
193.3	0.001	200	0	1	0
193.4	0.001	200	0	1	0

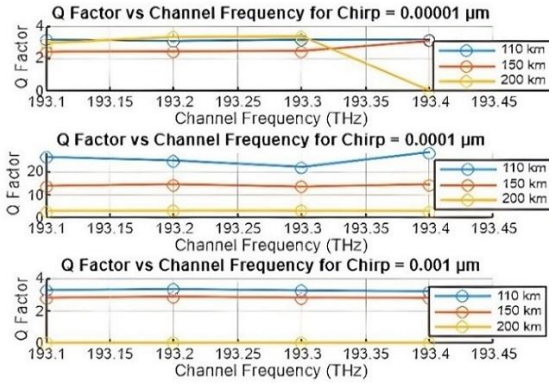

Figure 11. Q-factor variation with channel frequency for chirp parameters of 0.00001 µm, 0.0001 µm, and 0.001 µm over 110, 150, and 200 km SSMF in a 4-channel DWDM system

In the 4-channel DWDM system, performance was strongly influenced by the chirp value, channel frequency, and transmission distance. A chirp of 0.0001 µm yielded the best results, achieving an average Q-factor of 25.0765 with a BER of 1.271×10^{-105} at 110 km, and maintaining robust performance with an average Q-factor of 13.84 and a BER of 5.63×10^{-41} at 150 km. At 200 km, performance declined to an average Q-factor of 2.817 and a BER of 1.91×10^{-3}, underscoring the importance of precise chirp optimization for long-haul optical links.

4.5. Assessment of uniform fiber Bragg grating and apodised chirped fiber Bragg grating in single-, 4-, and 8-channel dense wavelength division multiplexing systems

This section presents a comparison between UFBG and ACFBG for CD compensation in single-, 4-, and 8-channel DWDM systems over SSMF spans of 110 km and 150 km, at an input power of 10 dBm and an FBG length of 30 mm, as illustrated in Figure 12. The evaluation emphasizes Q-factor and BER as the key performance metrics, with the overall results summarized in Table 7. To visually illustrate the performance differences, Figure 12(a) compares the Q-factor of the 4-channel system using UFBG and ACFBG across channel frequencies from 193.1 THz to 193.4 THz at a fiber length of 150 km, while Figure 12(b) presents the corresponding BER comparison. Similarly, Figure 12(c) displays the Q-factor comparison for the 8-channel system across channel frequencies from 193.1 THz to 193.8 THz at a fiber length of 150 km, and Figure 12(d) presents the BER performance for the same 8-channel configuration.

Table 7. Performance comparison of UFBG and ACFBG in single-, 4-, and 8-channel systems

Configuration	Fiber length (km)	Channel count	UFBG Q-factor	UFBG BER	ACFBG Q-factor	ACFBG BER
Single-channel	110	193.4	4.33992	7.12E-06	38.7341	0
Single-channel	150	193.4	0	1	16.5859	4.41E-62
4-channel	110	193.1	3.1643	0.0006524	25.9996	2.39E-149
		193.2	3.16521	0.000643	24.498	7.39E-133
		193.3	3.08486	0.0008184	21.7288	5.08E-105
		193.4	3.18093	0.0006126	28.0797	8.51E-174
4-channel	150	193.1	2.80073	0.0023997	13.586	2.39E-42
		193.2	2.87327	0.0019086	14.2489	2.25E-46
		193.3	2.76868	0.0025538	13.2495	2.23E-40
		193.4	2.73466	0.0028494	14.256	2.04E-46
8-channel	110	193.1	3.0775	0.0008324	9.00233	8.31E-20
		193.2	3.20374	0.0005821	8.845	3.40E-19
		193.3	3.13999	0.0006817	8.70447	1.11E-18
		193.4	2.79252	0.0019737	8.22649	6.84E-17
		193.5	3.07676	0.0008539	8.57049	3.58E-18
		193.6	3.00492	0.0010987	8.68256	1.31E-18
		193.7	3.05889	0.0009103	9.5362	4.80E-22
		193.8	3.06045	0.0008787	9.00566	6.92E-20
8-channel	150	193.1	2.70725	0.0030742	6.08178	4.92E-10
		193.2	3.02362	0.0012239	6.54431	2.55E-11
		193.3	2.69948	0.0031782	6.45385	4.34E-11
		193.4	2.55692	0.0045829	7.16206	3.40E-13
		193.5	2.72651	0.0029286	7.75014	3.78E-15
		193.6	2.72461	0.0030406	7.9549	7.52E-16
		193.7	2.73371	0.0028984	9.00981	8.70E-20
		193.8	2.81966	0.0022143	9.55403	5.39E-22

For the single-channel system at 193.4 THz over 110 km, UFBG delivers limited performance with a Q-factor of about 4.34 and BER of ~7.12×10^{-6}, whereas ACFBG achieves a significantly higher Q-factor of 38.73 and error-free transmission with BER=0. At 150 km, UFBG completely fails (Q-factor=0, BER=1), while ACFBG sustains strong performance with a Q-factor of ~16.59 and an ultra-low BER of 4.41×10^{-62}.

For the 4-channel DWDM system over 110 km, UFBG delivers low Q-factors (3.16–3.18) and relatively high BER (~10^{-4}), whereas ACFBG achieves much higher Q-factors (26–28) and ultra-low BERs (~10^{-174}), indicating effective dispersion and crosstalk suppression. At 150 km, UFBG's performance worsens, but ACFBG remains robust with Q-factors between 13.6 and 14.3 and BERs down to 10^{-46}.

In the 8-channel DWDM system, UFBG provides limited dispersion tolerance at 110 km with Q-factor ~3.07, and BER ~10^{-4}, while ACFBG shows strong performance with Q-factor ~9, and BER <10^{-20}. At 150 km, UFBG degrades further with Q-factor ~(2.7–2.8), and BER >10^{-3}, but ACFBG continues to operate effectively, maintaining Q-factors between 6 and 9.5 and BERs as low as 10^{-22}, demonstrating superior dispersion management and high transmission fidelity across multiple channels and longer distances.

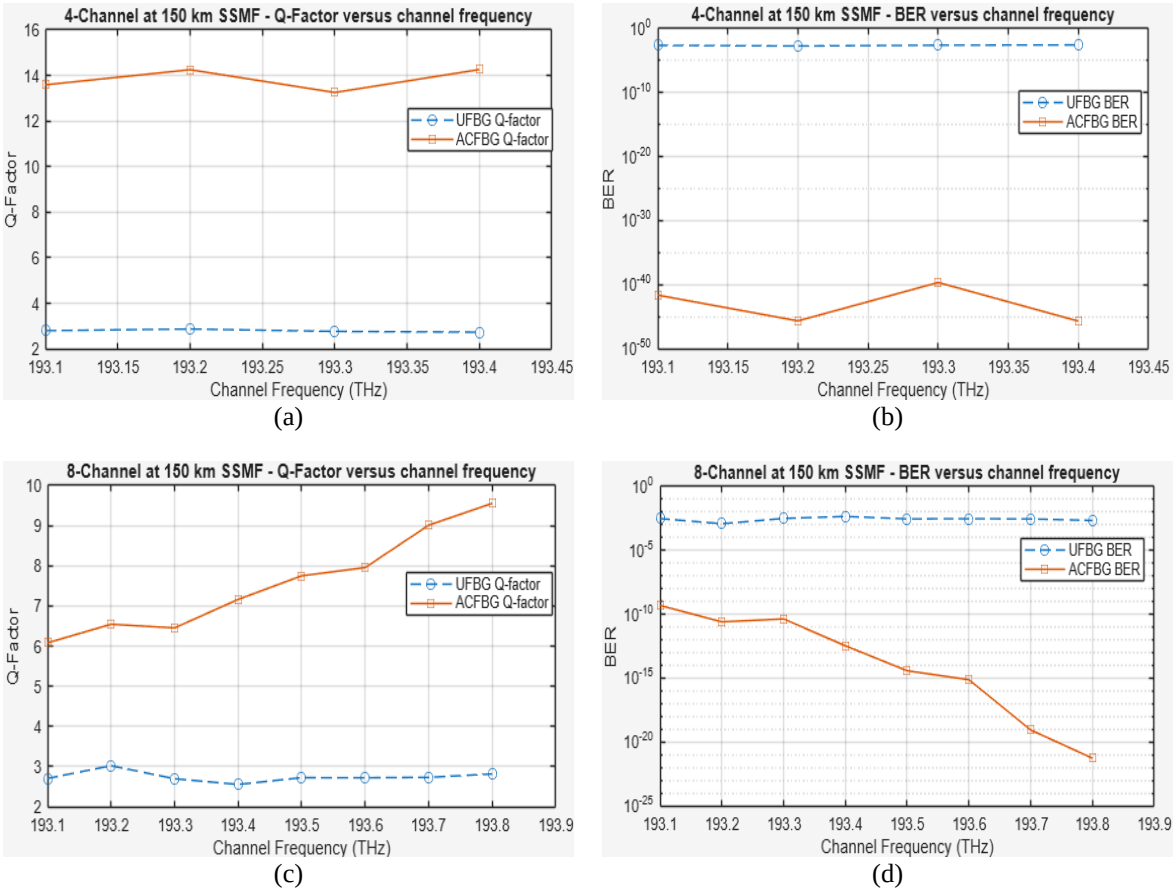

Figure. 12. Performance comparison of UFBG and ACFBG for 4- and 8-channel DWDM systems at 150 km SSMF; (a) Q-factor for 4-channel, (b) BER for 4-channel, (c) Q-factor for 8-channel, and (d) BER for 8-channel

Table 8 compares previous studies, where many relied on CFBG–DCF combinations, shorter spans (<110 km), or non-apodized gratings with lower performance. The proposed system achieves a higher Q-factor and lower BER using only an LDOC-based Gaussian-ACFBG, thereby reducing system complexity and cost.

Table 8. Evaluation of the proposed work against existing research findings

Ref.	Study/accomplishment	SSMF length (km)	CFBG length (mm)	Q-factor	BER
[5]	10 Gbps single-channel transmission with EDFA and uniform ACFBG for DC	150	45	12.7412	1.63383×10^{-37}
[11]	CD compensation for single-channel long-haul optical links using Gaussian ACFBG s combined with DCF	100	8	12.48	3.15×10^{-45}
[19]	Dispersion management using linear chirped FBG and tanh apodisation for a single-channel transmission	40	6	29.554	9.3407×10^{-182}
[21]	Coarse wavelength division multiplexing (CWDM) with 4-channel UFBG for DC	100	Not available	8.04225	1.60×10^{-16}
[23]	Analysis of 10 Gbps signals in a single-channel tanh ACFBG for DC	100	6	2.39784	7.32×10^{-3}
[24]	Analysed a 4-channel DWDM optical system using uniform apodisation, linear CFBG as DC	100	90	12.173	1.82×10^{-34}
[26]	Power budget reduction and performance enhancement in WDM systems using a novel FBG apodization function at 10 Gbps	110	50	8.36	3.13×10^{-17}
[28]	Hamming-ACFBG for post-DC in WDM system	110	50	8.27	6.46×10^{-17}
Proposed work	LDOC-based Gaussian-apodized linear CFBG for DC in a single-channel system at 10 Gbps	180	30	7.04	9.81767×10^{-13}
		150	30	16.5859	4.40737×10^{-62}
	4-channel DWDM system (average) at 10 Gbps	150	30	13.8351	5.57095×10^{-41}
	8-channel DWDM system (average) at 10 Gbps	150	30	7.56386	7.7597×10^{-11}

5. CONCLUSION

This study evaluates the performance of single- and multi-channel DWDM optical transmission systems operating at 10 Gbps. To mitigate CD, a LDOC scheme is employed. The scheme uses Gaussian-apodized linear CFBGs over SSMF spans ranging from 110 km to 210 km in single-, 4-, and 8-channel configurations. System performance is assessed in terms of Q-factor, BER, and eye height under varying fiber lengths, input power levels, and chirp parameters. Optimal single-channel performance was observed at 10 dBm input power with a 30 mm FBG length, supporting reliable transmission up to 180 km. At this distance, the system achieved a Q-factor of 7.04, BER of 9.82×10^{-13}, and eye height of 0.000233, meeting the acceptable thresholds of Q >6 and BER $\leq10^{-9}$. Among the tested chirp parameters, the linear chirp value of 0.0001 µm consistently yielded the best system performance across various fiber lengths and channel frequencies, thus confirming its suitability for robust DC in long-haul transmission. In the multi-channel scenario, the 4-channel DWDM system delivered Q-factors above 13 with extremely low BER, while the 8-channel DWDM system demonstrated good scalability, averaging a Q-factor of 7.56386, and average BER in the order of 10^{-11} at 150 km SSMF length, indicating robust performance even under higher channel densities. This study demonstrates that ACFBGs significantly outperform earlier approaches that struggled beyond 110 km or with higher channel counts, confirming their suitability for high-capacity DWDM systems in next-generation metro, backbone, and 5G/6G networks.

Recent fs laser inscription techniques, such as edge-weak-coupling and dual-path writing, enable precise fabrication of complex apodized chirped gratings. The validated parameters from this study (0.0001 µm linear chirp, 30 mm FBG length) provide practical design targets for such fabrication, supporting real-world integration. The next phase of this research will focus on experimental validation by fabricating ACFBGs and testing them on a 200 km fiber spool, including the impact of polarization and nonlinearities such as self-phase modulation (SPM) and cross-phase modulation (XPM). This will bridge the gap between simulation and practical deployment in DWDM networks.

ACKNOWLEDGMENTS

The author sincerely thanks Cambridge Institute of Technology, Bengaluru, and Visvesvaraya Technological University, Belagavi, for their valuable support and encouragement throughout this research. This research received no specific grant or contract from funding agencies in the public, commercial, or not-for-profit sectors.

FUNDING INFORMATION

No funding was received for this research.

AUTHOR CONTRIBUTIONS STATEMENT

This journal uses the Contributor Roles Taxonomy (CRediT) to recognize individual author contributions, reduce authorship disputes, and facilitate collaboration.

Name of Author	C	M	So	Va	Fo	I	R	D	O	E	Vi	Su	P	Fu
Kripa Kalkala Balakrishna	✓	✓	✓	✓	✓	✓	✓	✓	✓	✓			✓	
Gopalakrishna Murthy Chinnammahalli Ramappa				✓	✓			✓		✓	✓	✓		
Karthik Palani	✓			✓	✓	✓				✓	✓	✓	✓	

C : **C**onceptualization
M : **M**ethodology
So : **So**ftware
Va : **Va**lidation
Fo : **Fo**rmal analysis
I : **I**nvestigation
R : **R**esources
D : **D**ata Curation
O : Writing - **O**riginal Draft
E : Writing - Review & **E**diting
Vi : **Vi**sualization
Su : **Su**pervision
P : **P**roject administration
Fu : **Fu**nding acquisition

CONFLICT OF INTEREST STATEMENT

The authors report no conflicts of interest.

DATA AVAILABILITY

The authors confirm that the data supporting the findings of this study are available within the article.

REFERENCES

[1] M. L. Meena and R. K. Gupta, "Performance Estimation of Diverse Dispersion Compensation Modules for 16×10 Gbps," *Guangdianzi Jiguang/Journal of Optoelectronics Laser*, vol. 41, no. 6, pp. 861–872, 2022, doi: 10050086.2022.06.105.

[2] Z. Zaman, Y. Khan, and A. M. Khan, "Minimization of dispersion and non-linear effects in WDM based long-haul high capacity optical communication systems," *Journal of Optical Communications*, vol. 46, no. 2, pp. 457–463, 2025, doi: 10.1515/joc-2024-0086.

[3] T. Sarı and F. E. Durak, "Analyzing the Impact of EDFA Positioning on Signal Quality in DWDM," *Afyon Kocatepe University Journal of Sciences and Engineering*, vol. 25, no. 2, pp. 354–358, Mar. 2025, doi: 10.35414/akufemubid.1569525.

[4] A. H. Ali, S. Mutashar, and A. M. Hammadi, "Dispersion compensation of optical systems utilizing fiber Bragg grating at 15 Gbits/s," *Indonesian Journal of Electrical Engineering and Computer Science*, vol. 22, no. 1, pp. 369–378, Apr. 2021, doi: 10.11591/ijeecs.v22.i1.pp369-378.

[5] M. L. Meena and R. K. Gupta, "Design and comparative performance evaluation of chirped FBG dispersion compensation with DCF technique for DWDM optical transmission systems," *Optik*, vol. 188, pp. 212–224, Jul. 2019, doi: 10.1016/j.ijleo.2019.05.056.

[6] R. Adiati and S. Yani, "Comparing the Performance of Optical Communication Links using G.652 and G.655 Fiber in Python Packages," *Jurnal Pendidikan Fisika dan Teknologi*, vol. 10, no. 1, pp. 149–156, Jun. 2024, doi: 10.29303/jpft.v10i1.6935.

[7] B. Mukherjee, "WDM optical communication networks: Progress and challenges," *IEEE Journal on Selected Areas in Communications*, vol. 18, no. 10, pp. 1810–1824, Oct. 2000, doi: 10.1109/49.887904.

[8] G. Karpagarajesh, A. Blessie, and S. Krishnan, "Performance Assessment of Dispersion Compensation Using Fiber Bragg Grating and Dispersion Compensation Fiber Techniques," *Informacije MIDEM*, vol. 51, no. 4, pp. 215–223, Dec. 2021, doi: 10.33180/InfMIDEM2021.402.

[9] B. Gul and F. Ahmad, "1.28 Tbps DWDM optical network design using a dispersion compensating distributed Raman amplifier over S-band," *Opto-Electronics Review*, vol. 31, no. 2, pp. 146104–146104, Jun. 2023, doi: 10.24425/opelre.2023.146104.

[10] M. Chakkour, O. Aghzout, B. A. Ahmed, F. Chaoui, and M. El Yakhloufi, "Chromatic Dispersion Compensation Effect Performance Enhancements Using FBG and EDFA-Wavelength Division Multiplexing Optical Transmission System," *International Journal of Optics*, vol. 2017, pp. 1–8, 2017, doi: 10.1155/2017/6428972.

[11] I. Nsengiyumva, E. Mwangi, and G. Kamucha, "Performance Analysis of a Linear Gaussian- and tanh-Apodized FBG and Dispersion Compensating Fiber Design for Chromatic Dispersion Compensation in Long-haul Optical Communication Networks," *International Journal of Optics*, vol. 2022, no. 1, Jan. 2022, doi: 10.1155/2022/5734420.

[12] A. Wolf, A. Dostovalov, K. Bronnikov, M. Skvortsov, S. Wabnitz, and S. Babin, "Advances in femtosecond laser direct writing of fiber Bragg gratings in multicore fibers: technology, sensor and laser applications," *Opto-Electronic Advances*, vol. 5, no. 4, pp. 210055–210055, 2022, doi: 10.29026/oea.2022.210055.

[13] K. Grebnev, B. Perminov, T. T. Fernandez, A. Fuerbach, and M. Chernysheva, "Fluoride and chalcogenide glass fiber components for mid-infrared lasers and amplifiers: Breakthroughs, challenges, and future perspective," *APL Photonics*, vol. 9, no. 11, Nov. 2024, doi: 10.1063/5.0225887.

[14] Y. Willer *et al.*, "Apodized, plane-by-plane written chirped fiber Bragg gratings in polarization-maintaining fibers for dispersion control in all-fiber ultrafast lasers," in *Optical Components and Materials XX*, Mar. 2023, p. 6, doi: 10.1117/12.2647822.

[15] Q. Guo *et al.*, "Femtosecond laser fabricated apodized fiber bragg gratings based on energy regulation," *Photonics*, vol. 8, no. 4, p. 110, Apr. 2021, doi: 10.3390/photonics8040110.

[16] Y. Fan, W. Bao, C. Liao, and Y. Wang, "Chirped and tilted fiber Bragg gratings inscribed by femtosecond laser direct writing technology," in *Fourteenth International Conference on Information Optics and Photonics (CIOP 2023)*, Xi'an, China, Nov. 2023, p. 280, doi: 10.1117/12.3008141.

[17] H. Li *et al.*, "Robust femtosecond-written chirped and tilted fiber Bragg gratings for Raman filtering in multi-kW fiber lasers," *Optics Letters*, vol. 48, no. 14, p. 3697, Jul. 2023, doi: 10.1364/ol.493513.
[18] E. E. Elsayed, "Investigations on modified OOK and adaptive threshold for wavelength division multiplexing free-space optical systems impaired by interchannel crosstalk, atmospheric turbulence, and ASE noise," *Journal of Optics (India)*, Jun. 2024, doi: 10.1007/s12596-024-01929-4.
[19] F. Keti, "A New Proposed Model for Dispersion Compensation via Linear Chirped Fiber Bragg Grating," *Traitement du Signal*, vol. 41, no. 1, pp. 451–457, Feb. 2024, doi: 10.18280/ts.410139.
[20] B. A. Naguib, M. M. Ata, M. M. Alzalabani, and B. B. Yousif, "Performance evaluation and enhancement of apodized fiber Bragg grating for dispersion compensation," *AIP Advances*, vol. 11, no. 1, Jan. 2021, doi: 10.1063/5.0026190.
[21] A. H. Ali and R. K. Ibrahim, "Enhancement of single-mode optical fiber quality factor-bit error rate by using uniform fiber Bragg grating," *Indonesian Journal of Electrical Engineering and Computer Science*, vol. 27, no. 1, pp. 336–346, Jul. 2022, doi: 10.11591/ijeecs.v27.i1.pp336-346.
[22] C. Ghosh and V. Priye, "Dispersion compensation in a 24 × 20 Gbps DWDM system by cascaded chirped FBGs," *Optik*, vol. 164, pp. 335–344, Jul. 2018, doi: 10.1016/j.ijleo.2018.03.037.
[23] M. B. Hossain, A. Adhikary, and T. Z. Khan, "Performance Investigation of Different Dispersion Compensation Methods in Optical Fiber Communication," *Asian Journal of Research in Computer Science*, pp. 36–44, Apr. 2020, doi: 10.9734/ajrcos/2020/v5i230133.
[24] B. Yousif, S. S. Ahmed, and R. Waheed, "High Quality Factor and Dispersion Compensation Based on Fiber Bragg Grating in Dense Wavelength Division Multiplexing," *Optical Memory and Neural Networks (Information Optics)*, vol. 29, no. 3, pp. 228–243, Jul. 2020, doi: 10.3103/S1060992X20030078.
[25] Y. Mao, X. Yan, and W. Wang, "Principle and design of chirped fiber grating," *Journal of Physics: Conference Series*, vol. 1653, no. 1, p. 012011, Oct. 2020, doi: 10.1088/1742-6596/1653/1/012011.
[26] F. M. Mustafa, A. F. Sayed, and M. H. Aly, "A reduced power budget and enhanced performance in a wdm system: a new fbg apodization function," *Optical and Quantum Electronics*, vol. 54, no. 8, p. 471, Aug. 2022, doi: 10.1007/s11082-022-03876-5.
[27] G. P. Agrawal, *Fiber-Optic Communication Systems: Fourth Edition*. Wiley, 2010, doi: 10.1002/9780470918524.
[28] A. F. Sayed, F. M. Mustafa, A. A. M. Khalaf, and M. H. Aly, "Apodized chirped fiber Bragg grating for postdispersion compensation in wavelength division multiplexing optical networks," *International Journal of Communication Systems*, vol. 33, no. 14, Sep. 2020, doi: 10.1002/dac.4551.

BIOGRAPHIES OF AUTHORS

Kripa Kalkala Balakrishna obtained her B.E. in Electronics and Communication Engineering from SDM Institute of Technology, Ujire (2011) and M.Tech. in Microelectronics and Control Systems from NMAM Institute of Technology, Nitte (2013). She is currently a research scholar at the Department of Electronics and Communication Engineering, Cambridge Institute of Technology, Bengaluru, she previously served as an Assistant Professor at DSATM, Bengaluru, until 2022. Her research interests include photonics, optoelectronics, optical fiber communications, optical signal processing, and fiber sensors. She can be contacted at email: kripakb11@gmail.com.

Dr. Gopalakrishna Murthy Chinnammahalli Ramappa is an Associate Professor in the Department of Electronics and Communication Engineering at K S School of Engineering and Management, Bengaluru, with a Ph.D. in sensors for underwater applications and 22 years of teaching experience. His research interests include optical sensors, power electronics, communication systems, and embedded systems. He has published over 10 conference papers, numerous journal articles, and holds 1 design and 1 Indian patent (design granted). He has participated in several national and international workshops and seminars. He can be contacted at email: gopalakrishnamurthy.c.r@kssem.edu.in.

Dr. Karthik Palani completed B.E. (E&C) from Periyar University in 2004 and obtained M.E. in Applied Electronics in 2006 from Sathyabama Institute of Science and Technology (Deemed to be University). He obtained a Ph.D. from Dr. M.G.R. Educational and Research Institute (Deemed to be University) in 2013. He has 18 years of teaching experience in various engineering colleges. His research interests include mobile communication, underwater communication, underwater sensor networks, image processing, and machine learning applications. He has published over 50 conference papers, numerous journal articles, and holds 2 design and 2 Indian patents (design granted). An IEEE Senior Member, he is active in professional bodies and has attended many national and international workshops and seminars. He can be contacted at email: karthik.ise@cambridge.edu.in.